



Effects of extra amine sources on the permeability and separation properties of nanofiltration membranes prepared by polydopamine deposition

Jiaqi Li^a, Anqi Tang^b, Jingyu Lu^b, Peibin Zhang^b, Mingxia Shen^{a,*}, Liping Zhu^{b,**}

^aCollege of Mechanics and Materials, Hohai University, Nanjing 211100, China, Tel./Fax: +86 025 83786293; email: mxshen@hhu.edu.cn (M. Shen)

^bMOE Key Laboratory of Macromolecular Synthesis and Functionalization, Department of Polymer Science and Engineering, Zhejiang University, Hangzhou 310027, China, Tel./Fax: +86 571 87953011; email: lpzhu@zju.edu.cn (L. Zhu)

Received 14 August 2018; Accepted 22 December 2018

ABSTRACT

Mussel-inspired dopamine (DA) self-polymerization and deposition have exhibited great potential in the preparation of nanofiltration (NF) membranes with polydopamine (PDA) as a separation layer. It is believed that tris(hydroxymethyl) aminomethane (Tris), a commonly used buffer in DA self-polymerization, is involved in the PDA formation as an extra amine source. In this work, to clarify the effects of extra amine sources on the performances of PDA NF membranes, three buffers, bis(ethylenediamine)copper (II) (CuEn), ethylenediamine (En), and Tris, were used as extra amine sources in the preparation of PDA NF membranes, respectively. The permeation and separation performances of these membranes were compared in detail. The corresponding mechanisms of PDA formation with different extra amine sources were proposed. It was found that in Tris buffer, required separation performances can be reached though the accumulation of large PDA aggregates which resulted in a thick PDA selective layer (about 195 nm). In contrast, in CuEn buffer, a thinner, more uniform, and smoother selective layer was created by the assembly of smaller PDA species. Under optimized conditions, the water flux of the PDA NF membranes fabricated with CuEn buffer reached $38.4 \text{ L m}^{-2} \text{ h}^{-1}$ under 0.4 MPa, which was nearly 2 times as high as those of the membranes fabricated with En and Tris buffers. And the rejection to MgCl_2 and polyethylene glycol 1000 reached 84.4% and 95.6%, respectively. In addition, the PDA selective layer showed good structural stability in long-term tests. This work brings new insights in the optimization of NF membranes prepared by PDA deposition.

Keywords: Polydopamine; Nanofiltration; Extra amine sources; Deposition; Enhanced permeability

1. Introduction

The demand for highly efficient separation is urgent in chemical, energy, and environmental fields [1,2]. Membrane science has attracted much attention due to its comparative advantages of low cost, energy conservation, and environmental protection [3–5]. Nanofiltration (NF) membrane processes can effectively achieve molecular separation with low energy consumption in wastewater treatment, desalination, pharmaceutical and biotechnological

separation, and the food industry [6–13]. According to the separation mechanism of the NF process, the fabrication of NF membranes with an asymmetric structure that consists of a thin selective layer and a porous support substrate is consistently recommended [9,14]. There are many ways to construct selective layers onto a substrate, such as surface grafting, layer-by-layer deposition, and interfacial polymerization [15–20]. However, all these methods suffer from complicated preparation methods or weak interfacial adhesion between the selective layers and substrates. Therefore, a simple strategy for the construction of durable NF membranes is in great demand.

* Corresponding authors.

In recent years, catechol chemistry, which is inspired by the marine mussel adhesive phenomenon, has been extensively studied [21–26]. It was reported that dopamine (DA), a typical derivative of catechol, was able to form polydopamine (PDA) coatings on various substrates by a complicated oxidation, cross-linking, and self-assembly process under weakly alkaline conditions [27]. Because of its universal adhesion properties, PDA has been widely used for material surface modification in many fields [28]. PDA coatings based on mussel-inspired chemistry have been applied to membrane science in our previous works, including to improve hydrophilicity [29,30], to impart antifouling and antibacterial abilities [31–33], and to achieve further functionalization [34]. In addition, NF membranes were obtained by double-cycle PDA deposition on a polysulfone flat-sheet ultrafiltration membrane [35]. However, the conventional PDA deposition method suffers from a tedious preparation process and poor NF performances. Some efforts have recently been made to fabricate high-performance NF membranes by various PDA deposition methods. For example, an NF membrane was prepared on a polyethersulfone (PES) substrate via a multistep sequential process including the deposition of PDA, grafting of poly(ethylene imine) (PEI), and chemical cross-linking [16]. Lv et al. reported a strategy for fabricating NF membranes via the co-deposition of PDA and PEI followed by cross-linking with glutaraldehyde [36]. In addition, poly(vinyl alcohol) could be used in the co-deposition with PDA to prepare NF membranes [37]. These methods provided a selective layer with large pores resulting from the relatively large PDA aggregates; these pores, however, are not conducive to fine separation. Thus, most deposited PDA layers need to be cross-linked to increase the density of the structure of the selective layer. However, this process makes the separation aperture uncontrollable. Therefore, one-step methods for the preparation of controllable PDA NF membranes are in priority.

The reaction conditions influence the formation, aggregation, and deposition of PDA, which further affect the construction of a selective layer in NF membranes [38–40]. It has been reported that PDA aggregates are built on a monomer-polymer growth regime rather than a polymer-polymer one [41,42]. Small DA oligomer chains rapidly aggregate to form distinct entities that gradually grow to form larger aggregates. As previously reported, the growth of PDA aggregates can be efficiently controlled by experimental factors [40]. DA quinone, which governs covalent and noncovalent interactions, is the critical control point in the pathway. Nucleophiles such as amino group-containing tris(hydroxymethyl) aminomethane (Tris) in the medium could react with DA quinone by a nucleophilic addition reaction. As a buffer that is widely used for PDA deposition, Tris not only exerts a buffering effect but also is introduced into the PDA assembly process as an extra amine source, which affects the aggregation of DA oligomers and further affecting the size and shape of the resulting PDA aggregates [41]. PDA deposition is greatly influenced by extra amine sources [41–43]. However, the effect of buffers as extra amine sources on PDA deposition and the fabrication of PDA NF membranes have been rarely investigated. In our previous work, it was found that ethylenediamine (En), as an extra amine source buffer, was possibly involved in the

assembly of PDA, which changed the pathway of aggregation [43]. In addition, bis(ethylenediamine)copper (II) (CuEn), a metal complex of En that continuously releases En and Cu^{2+} , is also a potential amine source buffer and cross-linker used in PDA deposition. In this work, we intend to create PDA NF membranes with adjustable and controllable performances by the selection of extra amine sources in buffers. The effects of amine source (Tris, En, CuEn) on the permeation and separation performances of PDA NF membranes were investigated in detail. The pore size distribution, surface chemistry, and physical morphology of the prepared PDA NF membranes were characterized, and the mechanisms of PDA formation and deposition with different extra amine sources were proposed.

2. Experimental

2.1. Materials and Reagents

PES flat-sheet ultrafiltration (molecular weight cutoff at 10 kDa) membranes were purchased from Beijing Separation Equipment (China). Dopamine hydrochloride and CuEn hydroxide solution were purchased from Sigma-Aldrich (China) and used as received. Magnesium chloride (MgCl_2), magnesium sulfate (MgSO_4), sodium sulfate (Na_2SO_4), sodium chloride (NaCl), hydrochloric acid (HCl), En, Tris, and a series of polyethylene glycols (PEGs, molecular weight = 200–2,000 Da) were of analytical grade and obtained from the Sinopharm Chemical Reagent Co. (Shanghai, China). Vitamin B_{12} (VB_{12}) was obtained from the Aladdin Industry Co. (Shanghai, China). Ultrapure water was produced by a Millipore direct-Q system (USA).

2.2. Fabrication of PDA composite NF membranes

Dopamine hydrochloride (2 mg mL^{-1}) was dissolved in solution with different buffers of CuEn (30 mM), En (60 mM), and Tris (50 mM), respectively. The pH values of solution with CuEn and En were adjusted to 9 using hydrochloric acid with a concentration of 1 mol L^{-1} . And the pH value of solution with Tris was about 8.5. Typically, PES membranes were washed with ultrapure water three times and then immersed in the prepared solution shaken in an air oscillator at 25°C . The resulted PDA NF membranes were denoted as PES-CuEn-*n*, PES-En-*n*, and PES-Tris-*n* (where *n* is the immersion time (h)), respectively. Some PDA aggregates were also generated in the DA solutions and were collected by centrifugation. Afterward, the prepared membranes were washed with ultrapure water by vibration to remove the unreacted DA and buffer.

2.3. Characterizations of NF membranes and PDA aggregates

The surface chemistry of the PES substrate and the PDA NF membranes was tested by X-ray photoelectron spectroscopy (XPS; PHI 5000C ESCA system, USA) with Mg *K* α excitation radiation ($h\nu = 1,253.6 \text{ eV}$). The surface morphologies were observed by field emission scanning electron microscopy (FESEM; Hitachi S-4800, Japan) and atomic force microscopy (AFM; SPI3800N, Seiko Instrumental, Japan). AFM images were recorded in tapping mode with silicone tip cantilevers having a force constant

of 40 mN cm⁻¹ and were scanned in a 1 μm × 1 μm area. Root-mean-square roughness values (R_q) were calculated to express the surface roughness. Dynamic light scattering (DLS, Brookhaven, USA) and transmission electron microscopy (TEM, JEM1200, Japan) were employed to measure the sizes and morphologies of PDA aggregates in solution. After a certain reaction time, the pH value of the corresponding PDA solution was adjusted to 6 by 1 mol L⁻¹ of HCl to stop the reaction, and the solution was diluted 20 times before the test. The PDA aggregates were denoted as CuEn-*n*, En-*n*, and Tris-*n*, where *n* is the reaction time (h).

2.4. Separation performance tests and stability evaluation of PDA NF membranes

NF performance tests were carried out under 0.4 MPa pressure using a dead-end solvent-resistant stirred cell (Millipore Co., USA) with an effective area of 15 cm². The pressure in the stirred cell was controlled by the pressure regulator, which was connected to the atmosphere cylinder. All membranes were pre-pressured at 0.5 MPa with ultrapure water as the feed for 0.5 h before tests. The water flux (F , L m⁻² h⁻¹) was calculated using

$$F = \frac{V}{A \times t} \quad (1)$$

where V is the volume of permeate (L) during the operating time t (h) and A is the membrane area (m²).

After water permeation measurements, different salts (MgCl₂, MgSO₄, Na₂SO₄, and NaCl), VB₁₂, and PEG solutions were used as the feed solution to evaluate the separation performance, whose concentrations were 0.01 mol L⁻¹, 0.05 g L⁻¹, and 0.3 g L⁻¹, respectively. The salt concentration was measured by an electrical conductivity meter (DDS-11A, Shanghai Leici Instrument, China), VB₁₂ by a UV/vis spectrophotometer (UV5500-PC, Shanghai Jingke Instrument, China), and PEGs by a total organic carbon analyzer (Analytik Jena Multi N/C 3000, Jena, Germany). The rejection ratio (R , %) of the solute was calculated by

$$R = 1 - \frac{C_p}{C_f} \times 100\% \quad (2)$$

where C_p and C_f represent the solute concentrations in permeate and feed, respectively.

The pore size distribution of the PDA NF membranes was calculated by a solute transport method on rejections of PEGs with different molecular weights [44,45]. The mean effective pore diameter (μ_p) and the geometric standard deviation (σ_p) can be calculated by curve fitting. The pore size distribution can be expressed by the probability density function in the following equation:

$$\frac{dR(d_p)}{d(d_p)} = \frac{1}{d_p \ln \sigma_p \sqrt{2\pi}} \exp \left[-\frac{(\ln d_p - \ln \mu_p)^2}{2(\ln \sigma_p)^2} \right] \quad (3)$$

where d_p is the membrane pore size.

In this study, the long-term stability of the membrane was evaluated by a laboratory-scale cross-flow filtration apparatus at a constant flow rate of 0.5 L min⁻¹ for 72 h. In the test, 0.01 mol L⁻¹ MgCl₂ aqueous solution was used as feed solution at room temperature, and the transmembrane pressure was 0.4 MPa. The water flux and rejection of membranes were accordingly recorded every 4 h. All reported results were repeated at least three times.

3. Results and discussion

3.1. Membrane performances

The effects of PDA deposition time with three amine source buffers (CuEn, En, and Tris) on the performances of PDA NF membranes were investigated. When different amines are used, the PDA selective layers may show different electric charges, which will affect the salt rejections of NF membranes [46]. Therefore, we used a neutral molecule (VB₁₂) as the solute of feed solution to characterize the separation performances of the PDA selective layers. As shown in Figs. 1(a)–(c), the water flux and rejection of the PDA NF membranes exhibit almost the same trends even though the extra amine sources are different. With increasing deposition time, the thickness of the PDA selective layer increases and the flux decreases. It is well known that a longer deposition time means more complete deposition. With PDA deposition, the defects in the selective layer are reduced by the accumulation of PDA aggregates, causing the rejection to increase first and then remain at a stable level. In particular, the PDA in the CuEn buffer can quickly be deposited on the PES substrates to achieve the optimal separation performance at 3 h (Fig. 1(a)). In contrast, it takes 4 and 8 h for those membranes prepared in En and Tris buffers to achieve optimal separation performance, respectively (Figs. 1(b) and (c)). In this study, representative PDA NF membranes, PES-CuEn-3, PES-En-4, and PES-Tris-8, were used to study the PDA selective layers fabricated in three different extra amine source buffers. In particular, the water flux of PES-CuEn-3 is approximately two times as high as those of PES-En-4 and PES-Tris-8, whereas all membranes have similar VB₁₂ rejection values (Fig. 1(d)). Obviously, PDA can quickly form a selective layer on the PES substrate in CuEn buffer and achieve excellent permeability.

Additionally, the salt rejection performances of the PDA NF membranes were investigated. To study the influence of different extra amine sources on the electric charges of the PDA NF membranes, rejection tests with different salts at a concentration of 0.01 mol L⁻¹ were carried out (Fig. 2). Based on the Donnan effect and salt rejection performances, the degree of positive charge of the NF membranes follows the order PES-CuEn-3 > PES-En-4 > PES-Tris-8, which may be attributable to the positively charged amino groups of En and the neutrally charged hydroxyl groups of Tris [46]. In summary, PES-CuEn-3 and PES-En-4 were positively charged membranes, while PES-Tris-8 tended to be electrically neutral.

In previous reports, PDA-based coatings, including those co-deposition ones, as the selective layers of NF membranes have been studied in detail. Typically, the performance of NF membrane prepared by PDA deposition in different systems are compared in Table 1. It can be seen that our membranes

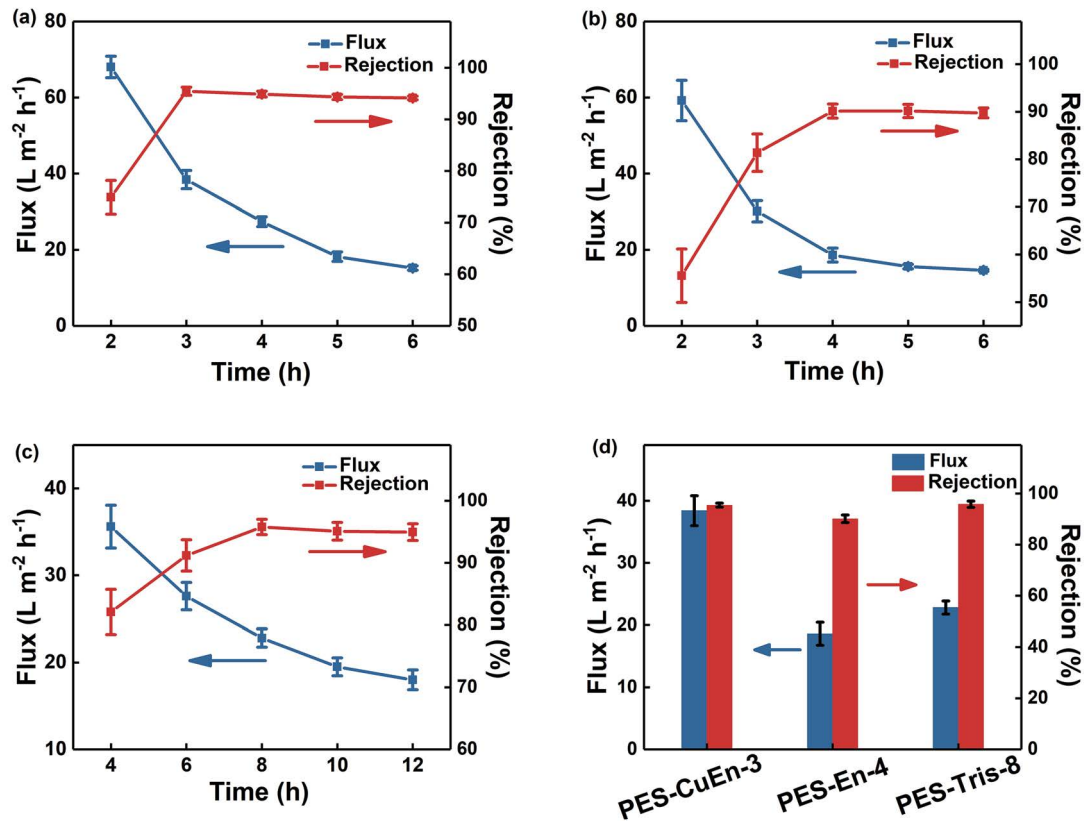


Fig. 1. Water flux and VB_{12} rejection of the PDA NF membranes fabricated in (a) CuEn, (b) En, (c) Tris buffers with different deposition times, and (d) Comparison of representative membranes.

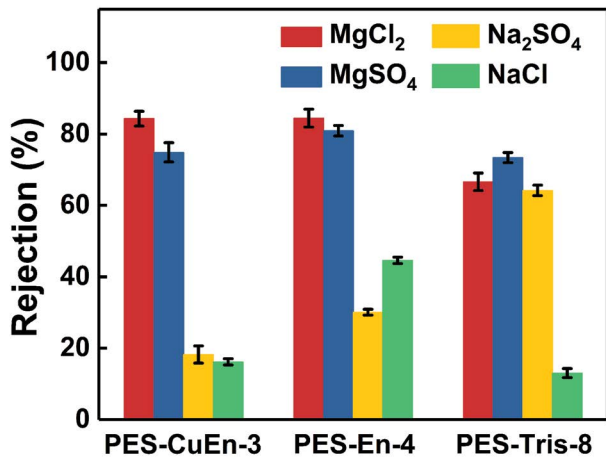


Fig. 2. Salt rejection performances of the PDA NF membranes. All salt solution concentrations are $0.01\ mol\ L^{-1}$.

possess relatively high permeability and rejection for divalent cation and low molecular weight cutoff.

3.2. Pore size distribution and stability of the NF membranes

Solute transport with PEG rejection tests was used to evaluate the pore size distribution of the studied

membranes. As depicted in Fig. 3(a), the three membranes show similar PEG rejection performance, with PES-CuEn-3 exhibiting a molecular weight cutoff of approximately 770 Da. The pore structure parameters of the studied membranes were calculated from the transport data with PEG solutes, as shown in Table 2. On the basis of the average pore size (μ_p) and geometric standard deviation (σ_p), the pore size distribution is shown in Fig. 3(b). This figure shows that the three kinds of PDA NF membranes have similar pore size distributions, which indicates that the pores in the PDA selective layer used for rejection are hardly affected by the involvement of extra amine sources.

The stability and durability of PES-CuEn-3 were examined by long-term NF tests for 72 h (Fig. 3(c)). The flux and rejection show little variation during long-term continuous testing. The PES-CuEn-3 membrane exhibits stable and excellent separation performance even after a long service time. This behavior makes the practical application of the PDA NF membranes possible.

3.3. Membrane surface chemistry and morphological characteristics

To confirm that PDA was deposited on the PES substrate and that extra amine sources were introduced into PDA, XPS was used to analyze the chemical composition of typical membrane surfaces. For the PDA NF membranes, the peaks of S 2p3 and S 2s disappear because of the coverage

Table 1
Nanofiltration performance of different composite membranes with PDA-based selective layers

NF membranes prepared by PDA deposition	Permeability (L m ⁻² h ⁻¹ bar ⁻¹)	rejection salts	Rejection (%)	Molecular weight cutoff (Da)	Reference
PDA deposition followed by PEI grafting	7.2	MgCl ₂	73.7	/	36
co-deposition of PDA and PEI followed by cross-linking	1.7	MgCl ₂	92	/	37
co-deposition of PDA and poly (vinyl alcohol)	13.6	Na ₂ SO ₄	94.2	/	38
PDA deposition triggered by CuSO ₄ /H ₂ O ₂	10.1	Na ₂ SO ₄	90	~1,000	40
PDA deposition in CuEn	9.6	MgCl ₂	84.4	~770	This work

/ represents no data in the reference.

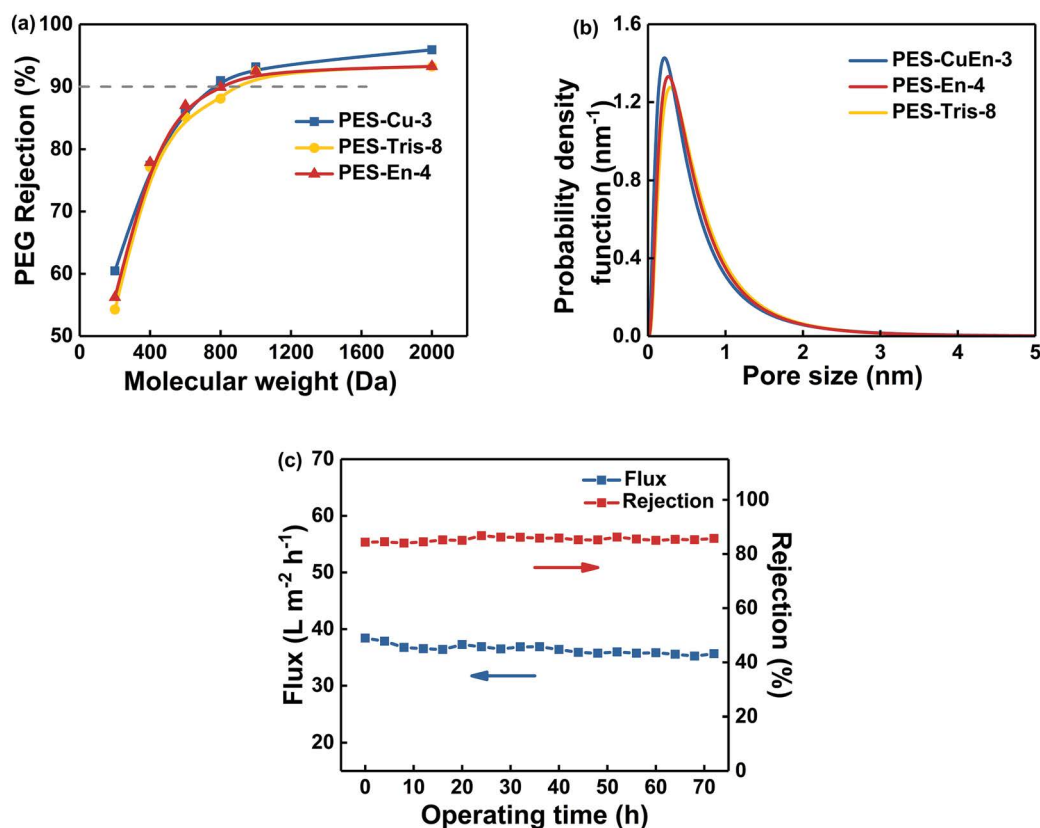


Fig. 3. (a) PEG rejection as a function of molecular weight for representative PDA NF membranes, (b) pore size distribution curves, and (c) effect of long-term NF tests on the water flux and MgCl₂ rejection of PES-CuEn-3. The concentration of PEGs of different molecular weights is 0.3 g L⁻¹. The MgCl₂ concentration is 0.01 mol L⁻¹.

with PDA layers (Fig. 4). This result indicates that the PDA was deposited onto the surface of the PES substrate. The appearance of an N 1s peak in the PES membrane may be due to the addition of a pore-forming agent in the fabrication process (Fig. 4). Compared with the original PES substrate, the PDA NF membrane shows an obvious increase in the N content, which is attributed to the N in PDA and the extra amine sources (Fig. 4 and Table 3). The N/C and N/O ratios of PES-En-4 and PES-CuEn-3 are significantly higher than those of PES-Tris-8, which is due to the involvement of

numerous En molecules in the assembly of PDA (Table 3). High-resolution XPS spectra show that C is mainly in the form of C–O/C–N, C–C/C=C, and a small part of C=O (<2%) was derived from quinone species (Fig. 5). The C–O/C–N ratio of PES-CuEn-3 (47.9%) is higher than that of PES-En-4 (32.8%). This result may be because there are more C–N bonds in PES-CuEn-3. The C–O/C–N value of PES-Tris-8 is 39.5%, which is due to the larger number of C–O groups in the Tris molecules involved in the assembly of PDA. In general, the extra amine sources were indeed introduced into the

Table 2
Parameters for membranes analyzed for PEG rejection

Membrane	μ_p (nm)	σ_p (nm)	Pore size cutoff (nm)
PES-CuEn-3	0.44	2.43	1.46
PES-En-4	0.51	2.26	1.83
PES-Tris-8	0.54	2.21	1.83

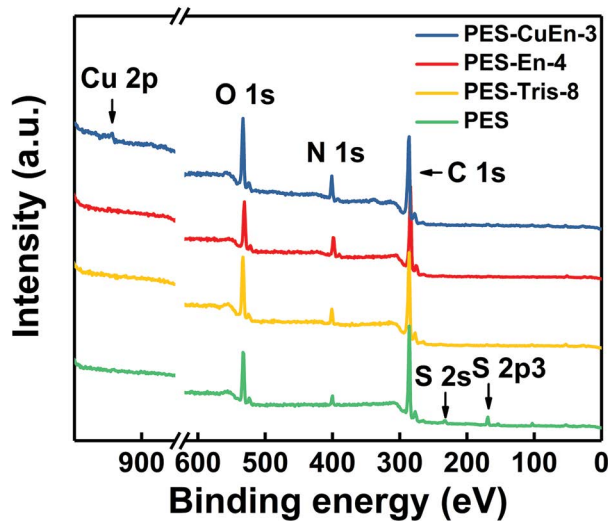


Fig. 4. Typical XPS wide scans for the investigated membranes.

Table 3
Surface chemical composition from XPS analysis of PES, PES-CuEn-3, PES-En-4, and PES-Tris-8

Sample	Atomic percentage (%, mole concentration)					N/C	N/O
	C	O	N	S	Cu		
PES	72.9	20.2	3.9	3.0	/	/	/
PES-CuEn-3	69.3	20.7	9.5	/	0.6	0.14	0.46
PES-En-4	72.7	16.2	11.1	/	/	0.15	0.69
PES-Tris-8	72.8	20.1	7.0	/	/	0.10	0.35

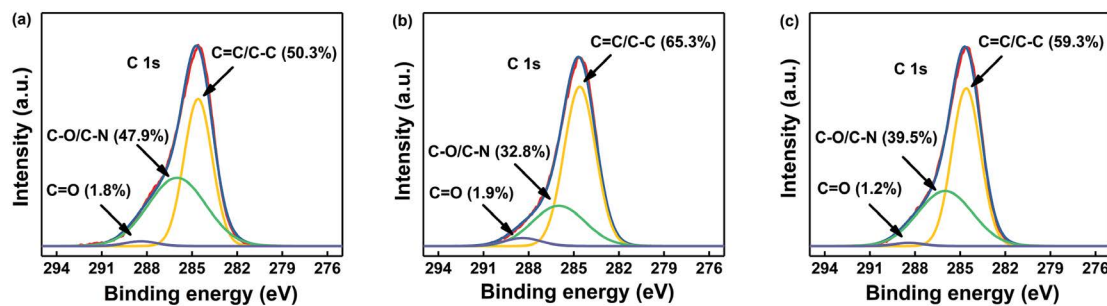


Fig. 5. High-resolution C 1s XPS spectra of different PDA NF membranes: (a) PES-CuEn-3, (b) PES-En-4, and (c) PES-Tris-8.

assembly of PDA, which is consistent with the salt rejection results of the studied membranes. The possible chemical mechanisms of three extra amine sources involved in the formation of PDA by Michael addition reaction or Schiff base reaction are shown in Fig. 6 [41,43].

In this study, FESEM was used to characterize the surface and cross-sectional morphologies of representative membranes (Fig. 7). As shown in the surface FESEM images of the membranes, the pristine PES membrane has a smooth surface, whereas the PDA NF membrane surfaces are comparatively rougher. The accumulation of PDA aggregates on the PES substrate is responsible for the rougher surface. The PES membrane surface is completely covered by a selective layer of accumulated PDA aggregates, as shown in the cross-sectional image. The PES-CuEn-3 membrane shows the thinnest selective layer (95 nm), while the thickness of the selective layers of PES-En-4 and PES-Tris-8 is 150 and 195 nm, respectively. Generally, the permeability is affected by the thickness of the selective layer. The thinner selective layer of PES-CuEn-3 is more conducive to higher flux. This explains why PES-CuEn-3 exhibits the best permeability. AFM analysis was also used to investigate the morphology of the membrane surfaces at nanoscale. The AFM images, along with the root-mean-square roughness (R_q) data, are shown in Fig. 7. The roughness of the PDA NF membrane surfaces follows the order PES-Tris-8 (9.89 nm) > PES-En-4 (8.34 nm) > PES-CuEn-3 (6.14 nm). Because the selective layer is fabricated by the accumulation of PDA aggregates, we speculate that roughness is related to the PDA nanoparticle size. A smooth selective layer may be provided by small PDA aggregates.

3.4. Analysis of PDA deposition process with different extra amine source buffers

To further study the reasons why the selective layer of PES-CuEn-3 was the thinnest among the membranes with similar pore size distributions, PDA aggregates were synthesized under the corresponding buffer conditions. DLS and TEM were used to evaluate the PDA aggregates. Figs. 8(a)–(c) show the mean size of three types of PDA aggregates at different reaction times. The mean size of PDA aggregates in CuEn buffer remains unchanged (~22 nm) even when the deposition time increases to 4 h (Fig. 8(a)). In contrast, the PDA aggregates in En or Tris buffer are larger after 2 h of reaction and grow with increasing reaction time (Figs. 8(b)

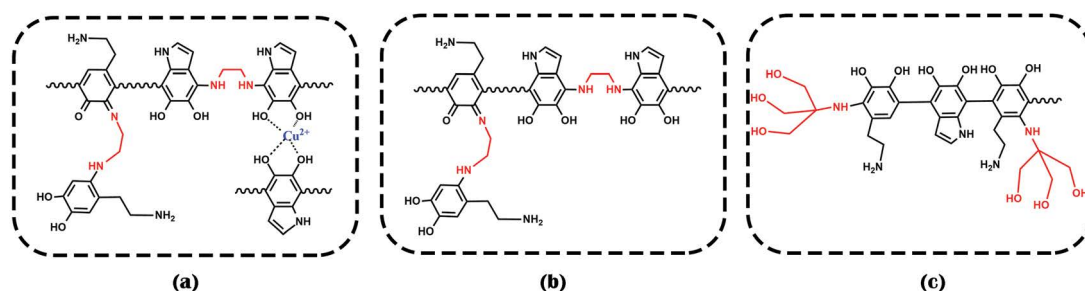


Fig. 6. Possible chemical mechanisms of PDA formation in (a) CuEn, (b) En, and (c) Tris buffer [41,43].

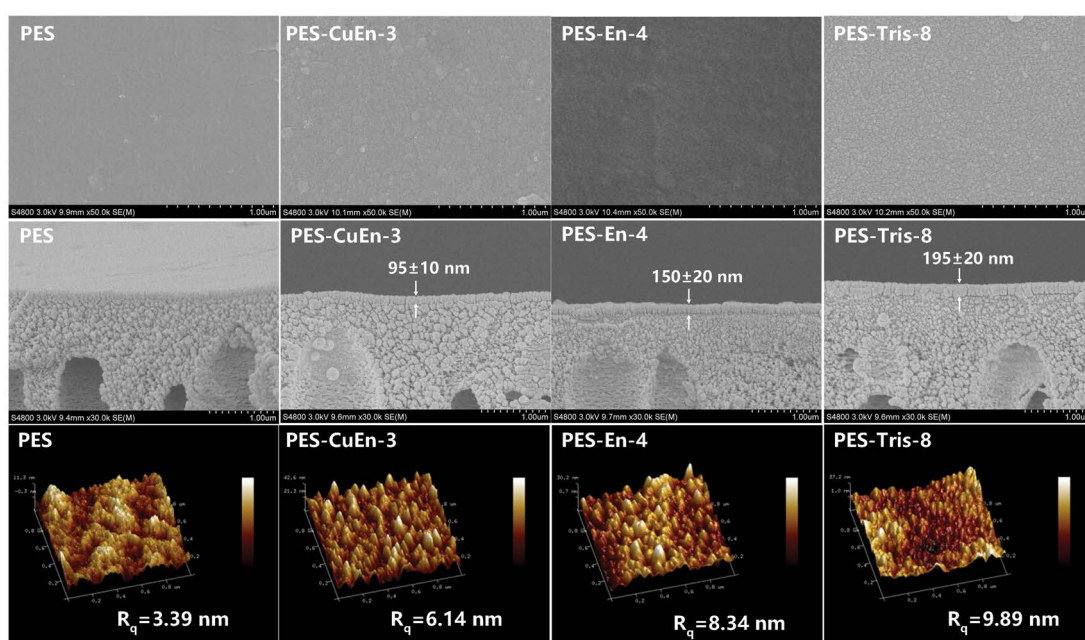


Fig. 7. Surface FESEM, cross-section FESEM, and AFM images of PES substrate and the PDA NF membranes fabricated with different buffers.

and (c)). Due to the involvement of many hydroxyl groups, the PDA aggregates exhibit stronger hydration in Tris buffer than in the other buffers, which allows them to form larger scale aggregates in water (Fig. 8(c)). Compared with those prepared in Tris buffer, PDA aggregates prepared in En buffer grow slower (Fig. 8(b)). In CuEn buffer, the En released slowly from CuEn can react with DA quinone by Michael addition or Schiff base reaction [43], and complexation between Cu^{2+} and the catechol groups occurs. For PDA oligomers, there may be a competitive relationship between aggregation and complexation. Therefore, the complexation of Cu^{2+} in CuEn buffer allows PDA aggregates to maintain a smaller size and hard to grow. This is a crucial factor in the formation of small and uniform PDA aggregates. The TEM images also indicate that the sizes of PDA aggregates in various buffers are different, which coincides well with the DLS results (Figs. 8(d)–(f)). Typically, CuEn-3 and En-4 are irregularly shaped, while Tris-8 is spherical. The spherical structure of Tris-8 is closely linked with strong hydration.

Obviously, because of the involvement of the buffer solute, the chemical structures of the PDA aggregates and the PDA assembly change, leading to PDA aggregating into different shapes.

Additionally, the order of membrane roughness is the same as the order of the size of PDA aggregates fabricated under corresponding conditions (Figs. 7 and 8(a)–(c)). This result also indicates that the accumulation of PDA on the substrate is closely related to the PDA nanoparticle size. In various PDA deposition systems for NF membrane preparation, it is a crucial issue that some big PDA aggregates are often generated and adhere to membrane surface, which may lead to membrane fouling. The use of CuEn as an extra amine source can suppress the aggregation of PDA oligomers, and thus, smoother PDA layer is formed on the substrate. This has the advantage of reducing membrane fouling.

Based on the performance of membranes and the various characterization results described above, we propose a mechanism for the deposition of PDA with different buffers

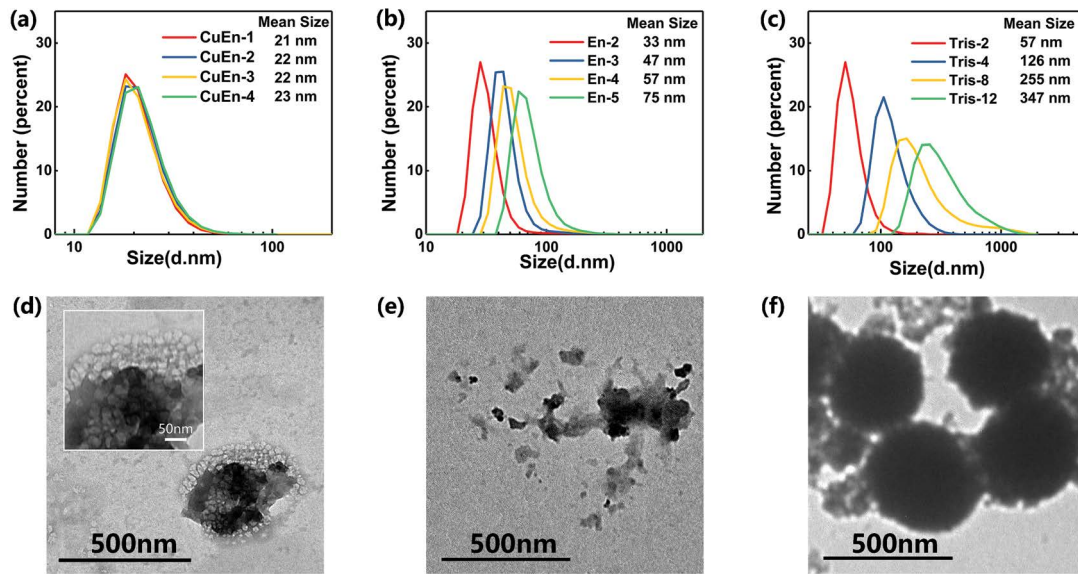


Fig. 8. DLS results of PDA aggregates fabricated with (a) CuEn, (b) En, and (c) Tris buffer with time and TEM images of (d) CuEn-3, (e) En-4, and (f) Tris-8.

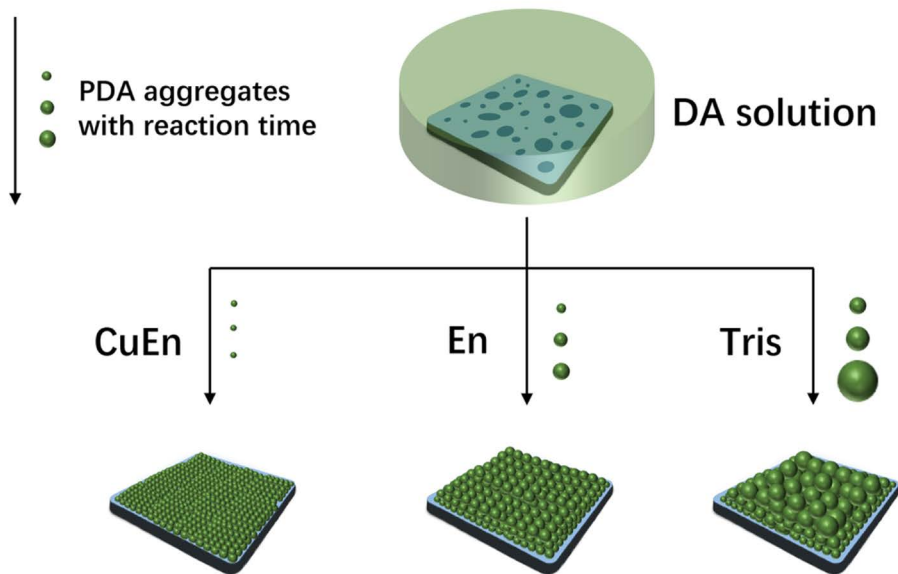


Fig. 9. Schematic diagram of PDA deposition on the substrate surface in three different extra amine source buffers.

on PES substrates (Fig. 9). In Tris buffer, the accumulation of large aggregates is not conducive to the construction of a compact selective layer, which means that it takes a longer time (8 h) to form a thicker layer (195 nm) to achieve optimal selective performance. In contrast, in CuEn buffer, small and uniform PDA aggregates were obtained and assemble into a thin, uniform, and smooth layer. This explains why PES-CuEn-3 can be rapidly deposited and exhibit better permeation performance than the other membranes. In summary, the formation, aggregation, and growth of PDA can be affected by extra amino sources, and PDA deposition can be controlled by the addition of different extra amine

sources. Undoubtedly, CuEn is an excellent buffer system for the construction of high-performance NF membranes.

4. Conclusions

The composite NF membranes with PDA as selective layers were successfully fabricated by the PDA deposition in three different buffers. Thin and compact PDA selective layers were rapidly constructed by small and uniform PDA aggregates in CuEn buffer, which is due to the fact that PDA aggregates can remain at a size of about 22 nm in CuEn buffer and no longer grow. In contrast, the accumulation of

large PDA aggregates is not conducive to the construction of a compact selective layer in Tris buffer, which means that it takes a longer time (8 h) to form a thicker layer (195 nm) to achieve optimal selective performance. Under optimized conditions, PES-CuEn-3 shows high rejection of PEG1000 and MgCl_2 (95.6% and 84.4%, respectively) and an excellent permeation flux of $38.4 \text{ L m}^{-2} \text{ h}^{-1}$, which is double that of the PDA NF membranes prepared with Tris or En buffer. The PES-CuEn-3 membrane shows a 770 Da molecular weight cutoff. The stability test demonstrates that PES-CuEn-3 is stable after 72 h of operation. The CuEn buffer system exhibits efficient potential for the construction of thin and uniform NF selective layers.

Acknowledgements

We are grateful for the financial supports from the National Natural Science Foundation of China (Grant No. 51573159, 51273176) and the Fundamental Research Funds for the Central Universities (Grant No. 2016QNA4032).

References

- [1] P. Angelini, T. Armstrong, R. Counce, W. Griffith, T. Lklason, G. Muralidharan, C. Narula, V. Sikka, G. Closset, G. Keller, *Materials for Separation Technologies, Energy and Emission Reduction Opportunities*, 2005.
- [2] D.S. Sholl, R.P. Lively, Seven chemical separations to change the world, *Nature*, 532 (2016) 435–437.
- [3] C.A. Solis, C.A. Velez, J.S. Ramirez, *Membrane technology: historical development*, *Entre Cienc. Ing.*, 10 (2016) 89–98.
- [4] M.R. Wiesner, S. Chellam, The promise of membrane technology, *Environ. Sci. Technol.*, 33 (1999) 360A–366A.
- [5] M.A. Shannon, P.W. Bohn, M. Elimelech, J.G. Georgiadis, B.J. Mariñas, A.M. Mayes, Science and technology for water purification in the coming decades, *Nature*, 452 (2008) 301–310.
- [6] W.J. Lau, A.F. Ismail, N. Misdan, M.A. Kassim, A recent progress in thin film composite membrane: a review, *Desalination*, 287 (2012) 190–199.
- [7] B.V. der Bruggen, Chemical modification of polyethersulfone nanofiltration membranes: a review, *J. Appl. Polym. Sci.*, 114 (2009) 630–642.
- [8] A.I. Schäfer, A.G. Fane, T.D. Waite, *Nanofiltration: Principles and Applications*, *Journal-American Water Works Association*, 11 (2005) 121–122.
- [9] A.W. Mohammad, Y.H. Teow, W.L. Ang, Y.T. Chung, D.L. Oatley-Radcliffe, N. Hilal, *Nanofiltration membranes review: recent advances and future prospects*, *Desalination*, 356 (2015) 226–254.
- [10] W.-J. Lau, A.F. Ismail, *Polymeric nanofiltration membranes for textile dye wastewater treatment: preparation, performance evaluation, transport modelling, and fouling control – a review*, *Desalination*, 245 (2009) 321–348.
- [11] J. Yin, B. Deng, *Polymer-matrix nanocomposite membranes for water treatment*, *J. Membr. Sci.*, 479 (2015) 256–275.
- [12] Y. Ji, W. Qian, Y. Yu, Q. An, L. Liu, Y. Zhou, C. Gao, Recent developments in nanofiltration membranes based on nanomaterials, *Chin. J. Chem. Eng.*, 25 (2017) 1639–1652.
- [13] J.R. Werber, C.O. Osuji, M. Elimelech, *Materials for next-generation desalination and water purification membranes*, *Nat. Rev. Mater.*, 1 (2016) 16018.
- [14] M. Paul, S.D. Jons, *Chemistry and fabrication of polymeric nanofiltration membranes: a review*, *Polymer*, 103 (2016) 417–456.
- [15] R. Zhang, S. Yu, W. Shi, W. Wang, X. Wang, Z. Zhang, L. Li, B. Zhang, X. Bao, A novel polyesteramide thin film composite nanofiltration membrane prepared by interfacial polymerization of serinol and trimesoyl chloride (TMC) catalyzed by 4-dimethylaminopyridine (DMAP), *J. Membr. Sci.*, 542 (2017) 68–80.
- [16] R. Zhang, Y. Su, X. Zhao, Y. Li, J. Zhao, Z. Jiang, A novel positively charged composite nanofiltration membrane prepared by bio-inspired adhesion of polydopamine and surface grafting of poly(ethylene imine), *J. Membr. Sci.*, 470 (2014) 9–17.
- [17] Y. Zeng, L. Wang, L. Zhang, J.Q. Yu, An acid resistant nanofiltration membrane prepared from a precursor of poly(s-triazine-amine) by interfacial polymerization, *J. Membr. Sci.*, 546 (2018) 225–233.
- [18] G.-R. Xu, X.-Y. Liu, J.-M. Xu, L. Li, H.-C. Su, H.-L. Zhao, H.-J. Feng, High flux nanofiltration membranes based on layer-by-layer assembly modified electrospun nanofibrous substrate, *Appl. Surf. Sci.*, 434 (2018) 573–581.
- [19] Z. Lin, Q. Zhang, Y. Qu, M. Chen, F. Soyekwo, C. Lin, A. Zhu, Q. Liu, LBL assembled polyelectrolyte nanofiltration membranes with tunable surface charges and high permeation by employing a nanosheet sacrificial layer, *J. Mater. Chem. A*, 5 (2017) 14819–14827.
- [20] Q. Zhang, L. Fan, Z. Yang, R. Zhang, Y. Liu, M. He, Y. Su, Z. Jiang, Loose nanofiltration membrane for dye/salt separation through interfacial polymerization with in-situ generated TiO_2 nanoparticles, *Appl. Surf. Sci.*, 410 (2017) 494–504.
- [21] J.H. Ryu, S. Hong, H. Lee, Bio-inspired adhesive catechol-conjugated chitosan for biomedical applications: a mini review, *Acta Biomater.*, 27 (2015) 101–115.
- [22] E. Faure, C. Falentin-Daudre, C. Jerome, J. Lyskawa, D. Fournier, P. Woisel, C. Detrembleur, Catechols as versatile platforms in polymer chemistry, *Prog. Polym. Sci.*, 38 (2013) 236–270.
- [23] S.K.M. Perikamana, J. Lee, Y.B. Lee, Y.M. Shin, E.J. Lee, A.G. Mikos, H. Shin, *Materials from mussel-inspired chemistry for cell and tissue engineering applications*, *Biomacromolecules*, 16 (2015) 2541–2555.
- [24] X. Zhang, Q. Huang, F. Deng, H. Huang, Q. Wan, M. Liu, Y. Wei, *Mussel-inspired fabrication of functional materials and their environmental applications: progress and prospects*, *Appl. Mater. Today*, 7 (2017) 222–238.
- [25] L. Li, W. Smitthipong, H. Zeng, *Mussel-inspired hydrogels for biomedical and environmental applications*, *Polym. Chem.*, 6 (2015) 353–358.
- [26] P.K. Forooshani, B.P. Lee, Recent approaches in designing bioadhesive materials inspired by mussel adhesive protein, *J. Polym. Sci. Polym. Chem.*, 55 (2017) 9–33.
- [27] H. Lee, S.M. Dellatore, W.M. Miller, P.B. Messersmith, *Mussel-inspired surface chemistry for multifunctional coatings*, *Science*, 318 (2007) 426–430.
- [28] M. Liu, G. Zeng, K. Wang, Q. Wan, L. Tao, X. Zhang, Y. Wei, Recent developments in polydopamine: an emerging soft matter for surface modification and biomedical applications, *Nanoscale*, 8 (2016) 16819–16840.
- [29] J. Jiang, L. Zhu, L. Zhu, B. Zhu, Y. Xu, *Surface characteristics of a self-polymerized dopamine coating deposited on hydrophobic polymer films*, *Langmuir*, 27 (2011) 14180–14187.
- [30] Z.-Y. Xi, Y.-Y. Xu, L.-P. Zhu, Y. Wang, B.-K. Zhu, A facile method of surface modification for hydrophobic polymer membranes based on the adhesive behavior of poly(DOPA) and poly(dopamine), *J. Membr. Sci.*, 327 (2009) 244–253.
- [31] J. Jiang, L. Zhu, L. Zhu, H. Zhang, B. Zhu, Y. Xu, *Antifouling and antimicrobial polymer membranes based on bioinspired polydopamine and strong hydrogen-bonded poly(n-vinyl pyrrolidone)*, *ACS Appl. Mater. Interfaces*, 5 (2013) 12895–12904.
- [32] J.-H. Jiang, L.-P. Zhu, H.-T. Zhang, B.-K. Zhu, Y.-Y. Xu, *Improved hydrodynamic permeability and antifouling properties of poly(vinylidene fluoride) membranes using polydopamine nanoparticles as additives*, *J. Membr. Sci.*, 457 (2014) 73–81.
- [33] J. Jiang, P. Zhang, L. Zhu, B. Zhu, Y. Xu, *Improving antifouling ability and hemocompatibility of poly(vinylidene fluoride) membranes by polydopamine-mediated ATRP*, *J. Mater. Chem. B*, 3 (2015) 7698–7706.
- [34] L.-P. Zhu, J.-H. Jiang, B.-K. Zhu, Y.-Y. Xu, *Immobilization of bovine serum albumin onto porous polyethylene membranes using strongly attached polydopamine as a spacer*, *Colloids Surf., B*, 86 (2011) 111–118.

- [35] X. Li, L. Zhu, J. Jiang, Z. Yi, B. Zhu, Y. Xu, Hydrophilic nanofiltration membranes with self-polymerized and strongly-adhered polydopamine as separating layer, *Chin. J. Polym. Sci.*, 30 (2012) 152–163.
- [36] Y. Lv, H.-C. Yang, H.-Q. Liang, L.-S. Wan, Z.-K. Xu, Nanofiltration membranes via co-deposition of polydopamine/polyethylenimine followed by cross-linking, *J. Membr. Sci.*, 476 (2015) 50–58.
- [37] T. Wang, H. Qiblawey, S. Judd, A. Benamor, M.S. Nasser, A. Mohammadian, Fabrication of high flux nanofiltration membrane via hydrogen bonding based co-deposition of polydopamine with poly(vinyl alcohol), *J. Membr. Sci.*, 552 (2018) 222–233.
- [38] S. Hong, Y.S. Na, S. Choi, I.T. Song, W.Y. Kim, H. Lee, Non-covalent self-assembly and covalent polymerization co-contribute to polydopamine formation, *Adv. Funct. Mater.*, 22 (2012) 4711–4717.
- [39] C. Zhang, Y. Lv, W.-Z. Qiu, A. He, Z.-K. Xu, Polydopamine coatings with nanopores for versatile molecular separation, *ACS Appl. Mater. Interfaces*, 9 (2017) 14437–14444.
- [40] N.F.D. Vecchia, R. Avolio, M. Alfè, M.E. Errico, A. Napolitano, M. d'Ischia, Building-block diversity in polydopamine underpins a multifunctional eumelanin-type platform tunable through a quinone control point, *Adv. Funct. Mater.*, 23 (2013) 1331–1340.
- [41] N.F.D. Vecchia, A. Luchini, A. Napolitano, G. D'Errico, G. Vitiello, N. Szekely, M. d'Ischia, L. Paduano, Tris buffer modulates polydopamine growth, aggregation, and paramagnetic properties, *Langmuir*, 30 (2014) 9811–9818.
- [42] M. d'Ischia, A. Napolitano, V. Ball, C.-T. Chen, M.J. Buehler, Polydopamine and eumelanin: from structure–property relationships to a unified tailoring strategy, *Acc. Chem. Res.*, 47 (2014) 3541–3550.
- [43] P. Zhang, A. Tang, B. Zhu, L. Zhu, H. Zeng, Hierarchical self-assembly of dopamine into patterned structures, *Adv. Mater. Interfaces*, 4 (2017) 1601218.
- [44] B. Van Der Bruggen, J. Schaep, D. Wilms, C. Vandecasteele, A comparison of models to describe the maximal retention of organic molecules in nanofiltration, *Sep. Sci. Technol.*, 35 (2000) 169–182.
- [45] S. Singh, K.C. Khulbe, T. Matsuura, P. Ramamurthy, Membrane characterization by solute transport and atomic force microscopy, *J. Membr. Sci.*, 142 (1998) 111–127.
- [46] J. Schaep, B. Van der Bruggen, C. Vandecasteele, D. Wilms, Influence of ion size and charge in nanofiltration, *Sep. Sci. Technol.*, 14 (1998) 155–162.